Approaching Charge Separation Efficiency to Unity without Charge Recombination

Sa Zhang,[1] Jianfeng Wang,[2] Shizheng Wen[2] Ming Jiang,[1] Haiyan Xiao,[1,*] Xiang Ding,[1] Ning Wang,[1] Menglu Li,[1] Xiaotao Zu,[1] Sean Li,[3] ChiYung Yam,[2] Bing Huang,[2,4,†] and Liang Qiao[1,‡]

[1]*School of Physics, University of Electronic Science and Technology of China, Chengdu 610054, China*
[2]*Beijing Computational Science Research Center, Beijing, 100193, China*
[3]*School of Materials, University of New South Wales, Sydney 2052, New South Wales Australia*
[4]*Department of Physics, Beijing Normal University, Beijing 100875, China*

Improving the efficiency of charge separation (CS) and charge transport (CT) is essential for almost all optoelectronic applications, yet its maximization remains a big challenge. Here we propose a conceptual strategy to achieve CS efficiency close to unity and simultaneously avoid charge recombination (CR) during CT in a ferroelectric polar-discontinuity (PD) superlattice structure, as demonstrated in $(BaTiO_3)_m/(BiFeO_3)_n$, which is fundamentally different from the existing mechanisms. The competition of interfacial dipole and ferroelectric PD induces opposite band bending in $BiFeO_3$ and $BaTiO_3$ sublattices. Consequently, the photoexcited electrons (e) and holes (h) in individual sublattices move forward to the opposite interfaces forming electrically isolated e and h channels, leading to a CS efficiency close to unity. Importantly, the spatial isolation of conduction channels in $(BaTiO_3)_m/(BiFeO_3)_n$ enable suppression of CR during CT, thus realizing a unique band diagram for spatially orthogonal CS and CT. Remarkably, $(BaTiO_3)_m/(BiFeO_3)_n$ can maintain a high photocurrent and large band gap simultaneously. Our results provide a fascinating illumination for designing artificial heterostructures toward ideal CS and CT in optoelectronic applications.

Photoelectron conversion relies on efficient light-matter interaction, including light absorption, charge separation (CS), and charge transport (CT). This process is not only of fundamental interest for condensed mater physics, but also crucial for the performance of state-of-art optoelectronics, photovoltaics (PVs), photodetectors, and artificial photosynthesis [1–5]. While light absorption depends strictly on a macroscopic static band gap of semiconductors, CS and CT are mostly sensitive to local electronic structure, Coulomb correlation, and dynamics of photoexcited carriers [6,7]. Several types of CS with different mechanisms have been proposed, i.e., traditional p-n junctions [8,9] [Fig. 1(a)] or emergent van der Waals (vdW) heterojunctions [10], and bulk photovoltaic (BPV) effects [Fig. 1(b)] [11–15]. However, the strong carrier recombination (CR) exists in all the existing CS mechanisms. For example, although the internal polarization of ferroelectrics facilitates CS, the large band gap and strong recombination limit the device efficiency. While different approaches are being explored to effectively reduce their band gap, i.e., epitaxial strain [16,17], doping [18,19], or phase transition [20], CR remains a problem.

Besides of the lack of ideal CS, another major obstacle is the realization of ideal CT to effectively suppress CR during the photoelectric conversion, which is restricted by the intrinsic band diagrams of p-n junctions [Fig. 1(a)] and BPV junctions [Fig. 1(b)]. For a p-n junction (or type-II

vdW heterojunction), the effectively spatial separation of electrons (e) and holes (h) is mainly realized during charge-generation process under internal built-in potentials, occurring in zone II (green color) with a weak recombination. However, after charge generation and when carriers enter a field-free transport zone (zones I and III), due to absence of built-in potentials, recombination significantly increases, resulting in coexistence of carrier generation and recombination (red-green mixed color). For a BPV junction, differing from the p-n junction, carriers are generated from the intrinsic topological Berry phase polarization, i.e., ferroelectricity, inside the material. Similar to the p-n junction, the e and h are always mixing, thus leading to intrinsic (domain) and extrinsic (domain boundary) recombination during both the generation and transport process (zones I and III). As a result, CS and CT always coexist and occur along the *same* direction in p-n and BPV junctions, making CR intrinsically unavoidable.

Here we propose a conceptually new mechanism to realize *orthogonal* charge separation and transport (OCST), which can fundamentally eliminate CR during CT. The basic idea is to realize a unique band diagram to maintain the spatial separation of carriers not only during charge generation, but also throughout the following transport process. Figure 1(c) illustrates such an ideal band diagram, exhibiting a peculiar potential gradient profile with separated energy valleys in valence band maximum
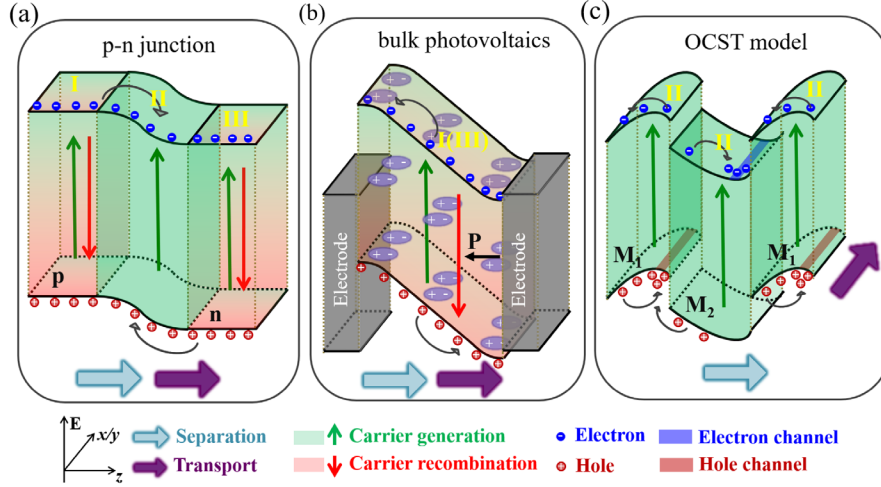
FIG. 1.   Schematic band diagrams for (a) conventional p-n junction model, (b) BPV model, and (c) OCST model. Charge generation and recombination coexist in (I) and (III) zones (mixed red-green color), while zone (II) is free of recombination (green color). M_1 and M_2 refer to two constituting materials of the interface or superlattice.

(VBM) and conduction band minimum (CBM), leading to the formation of spatially isolated channels for e (blue) and h (red) in two sublattices. In this case, CS and CT will occur in an orthogonal geometry, leading to substantially suppressed CR during transport process. Meanwhile, if the excited carriers can be confined in local regions, as shown in Fig. 1(c), a strong enhancement of photocurrent might be achieved simultaneously.

In this Letter, it is shown that the ideal OCST model can be realized in a simple oxide super-lattice with ferroelectric polar discontinuity (PD), as demonstrated in $(BaTiO_3)_m/(BiFeO_3)_n$ based on extensive first-principles calculations (see details of methods in Supplemental Material [21]). The interfacial PD in $(BaTiO_3)_m/(BiFeO_3)_n$ creates built-in potentials to separate VBM and CBM in different sublattices. Driving by the opposite band bending in different sublattices, the spatially separated e and h, generated by photoexcitation, move to opposite directions forming isolated conduction channels. Importantly, the unique OCST band diagram of $(BaTiO_3)_m/(BiFeO_3)_n$ can greatly suppresses CR during CT, leading to 2 orders of magnitude enhancement of photocurrent compared to that of pure $BiFeO_3$ system. Simultaneously, $(BaTiO_3)_m/(BiFeO_3)_n$ can achieve both high photocurrent and large band gap, fundamentally differing from the traditional semiconductors and providing a new diagram for broad optoelectronic applications, such as PVs, photodetection, or photosensors near visible-UV range.

Figure 2(a) shows a representative band structure for $(BaTiO_3)_2/(BiFeO_3)_2$, which is different from straightforward linear convolution of two bulk references (Supplemental Material, Fig. S1 [21]). The conduction band (CB) near Fermi level mainly comes from Fe and Bi orbitals of $BiFeO_3$, while the valence band (VB) is more

similar to that of $BaTiO_3$. Therefore, the VBM and CBM of $(BaTiO_3)_2/(BiFeO_3)_2$ locate in $BaTiO_3$ and $BiFeO_3$ sublattices, respectively, which is a general feature for the different choices of m and n (Fig. S2 [21]). The spatial separation of holes and electrons is attributed to the electronic reconstruction induced by interfacial PD, in analogy to polar catastrophe in polar-nonpolar oxide heterostructures [59,129–131]. In $(BaTiO_3)_m/(BiFeO_3)_n$ superlattice, the mismatch of valence electrons for a B-site cation (e.g., Ti^{4+} vs Fe^{3+}) along the [001] direction results in dipole mismatch between planes of BaO-TiO_2 and BiO-FeO_2 (Fig. S3 [21]), leading to the presence of built-in potential perpendicular to interface that can alter interface band alignment. The built-in potential is demonstrated by shift of VBM and CBM in Fig. 2(b) for a representative $(BaTiO_3)_4/(BiFeO_3)_{10}$. Significantly, the band edges for $BiFeO_3$ and $BaTiO_3$ layers show opposite energy moves, suggesting opposite built-in electric fields, leading to the spatial separation of holes and electrons. Furthermore, we notice that the CBM is not located at the interface but within top layers in $BiFeO_3$ [Fig. 2(b)], thus enabling spatially offset e conduction channel away from interface [see further discussions in Figs. 2(d) and 3].

This unique electronic structure is the direct consequence of multiple competing polarization mechanisms. As illustrated in Fig. 2(c), ferroelectric-polarization-induced electric field ($P_1 \sim 142$ and $P_2 \sim 103$ $\mu C/cm^2$ for $BiFeO_3$ and $BaTiO_3$ layers, respectively, in superlattice) and PD-induced electric field E_d (equivalent to $P_{dipole} \sim 32$ $\mu C/cm^2$ induced field) coexist in the superlattice. Driven by interface boundary requirement and ferroelectric domain wall energy minimization, the interfacial ferroelectric polarization difference creates an extra electrostatic field ($\Delta P = P_1$-P_2) that favors an opposite direction with existing E_d (Fig. S4 [21]). Furthermore, there is
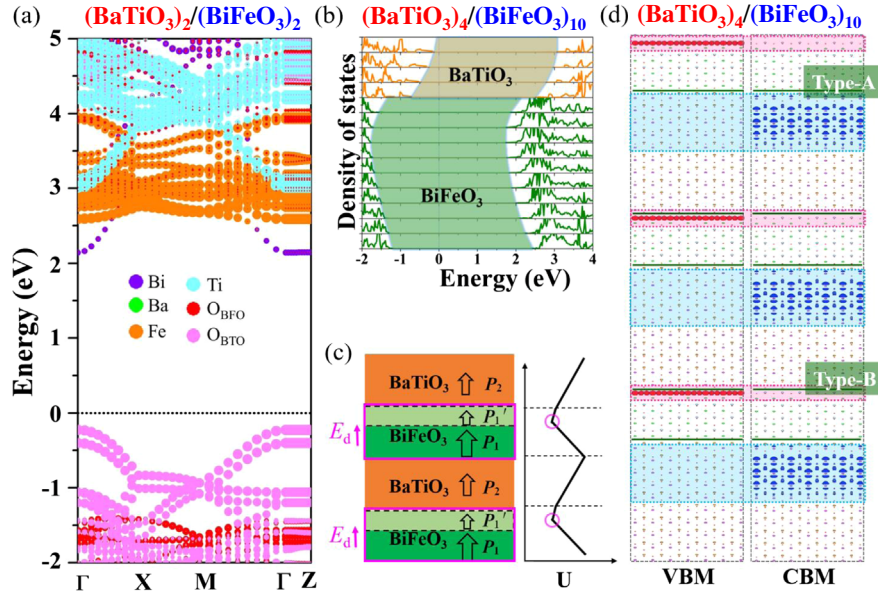
FIG. 2. (a) Band structure for $(BaTiO_3)_2/(BiFeO_3)_2$. (b) Layer-resolved DOS for $(BaTiO_3)_4/(BiFeO_3)_{10}$. (c) Schematic plot of ferroelectric polarizations and dipole-induced electric field (left) and electrostatic potential (U) along the superlattice direction (right). Hollow arrows are ferroelectric polarizations (P_1, P_2, and P_1'), and pink arrow is electric field induced by dipolar polarization (E_d). Interface structural relaxation in $BiFeO_3$ leads to $P_1' < P_1$. CBM in $BiFeO_3$ are marked by pink circles. (d) Charge density distributions at VBM (left) and CBM (right) for $(BaTiO_3)_4/(BiFeO_3)_{10}$.

spontaneous structural relaxations near $BaTiO_3/BiFeO_3$ interface (Figs. S5 and S6 [21]), leading to a reduced ferroelectric polarization (P_1') in $BiFeO_3$. As shown in Fig. 2(c), the interface relaxation effects can effectively shift the CBM away from interface (see more discussions in the Supplemental Material, Fig. S5 [21]). Similar potential gradient profile with CBM can be observed in all $(BaTiO_3)_m/(BiFeO_3)_n$ systems (Figs. S7 and S13 [21]).

The superlattices can exhibit strongly anisotropic e/h transport along the in-plane (IP) and out-of-plane (OOP) directions. A closer inspection of the CBM and VBM regions in Fig. 2(a) reveals bands are dispersive (i.e., small effective masses) along the IP direction, while bands along the OOP direction are very flat (i.e., huge effective masses) in a large energy region, similar to the vdW systems [132], which indicates e and h transport mainly occurs IP reflecting quantum confinement [133,134]. Especially compared with pure $BiFeO_3$ [Fig. S1(e) [21]]], the CBM of $BiFeO_3$ in superlattice shows much stronger anisotropic IP electron conductivity due to this confinement. It is emphasized that all superlattices with different m and n exhibit similar band dispersions for CBM and VBM (Fig. S2 [21]). Therefore, the interfacial built-in dipolar-mismatch-induced net dipole field, along with intrinsic ferroelectric polarization and spatially separated electronic structure, can largely hinder CT in $(BaTiO_3)_m/(BiFeO_3)_n$ along the OOP direction; e.g., the simulated IP photo-current of $(BaTiO_3)_4/(BiFeO_3)_4$ is at least 3 orders of magnitude larger than that of the OOP one, based on the first-principles photocurrent calculations (Fig. S8 [21]).

To visualize the spatial CS, taking $(BaTiO_3)_4/(BiFeO_3)_{10}$ as a typical example, we present its partial charge density distribution in real space in Fig. 2(d). It is seen that the superlattice contains two types of interfaces, i.e., types A and B. Meanwhile, the charge density of VBM and CBM states are located in $BaTiO_3$ (red-colored region) and $BiFeO_3$ (blue-colored region), respectively. Interestingly, only the $BaTiO_3$ layer next to the type-B interface offers the most significant contribution to the location of VBM charge density (Figs. S11 and S12 [21]). This interface-dominated VBM contribution is a direct consequence of built-in potential, which is layer dependent and only pushes the very interface layer (type-B interface) to VBM, giving rise to the accumulation of photoexcited h in this layer forming an h channel (light red box). Meanwhile, the CBM of $(BaTiO_3)_4/(BiFeO_3)_{10}$ is primarily localized near the type-A interface region with a 4 u.c. (unit cell) thickness, forming an e channel (light blue box). While in between e and h channels, the field creates a special region where both e and h are electrically forbidden, as the depletion channel, with thickness around 3–6 u.c. [Fig. 2(d)]. A similar charge density distribution, is general, found in other $(BaTiO_3)_m/(BiFeO_3)_n$ (Figs. S13–S15 [21]). It is clear that different degrees of e-h spatial separation can be tuned by the value of m (or n) in $(BaTiO_3)_m/(BiFeO_3)_n$ (see details in Supplemental Material [21]).

This peculiar distribution of e and h channels, along with unique built-in potential profile across interfaces, is expected to induce intriguing phenomena under photo-excitation. Again, using $(BaTiO_3)_4/(BiFeO_3)_{10}$ as an example, Fig. 3 presents its three-dimensional band
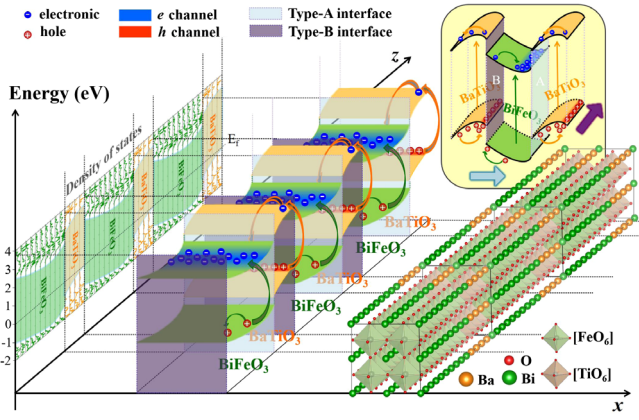
FIG. 3. Three-dimensional band structure combining both reciprocal energy space and real lattice space for $(BaTiO_3)_4/(BiFeO_3)_{10}$. Under photoexcitation, both $BaTiO_3$ and $BiFeO_3$ layers show intralayer excitation, then the built-in potential drives the generated e or h to drift to its own energy minima toward type-A or type-B interfaces. See text for more explanation.

diagram, combining both reciprocal energy space and real lattice space, to elucidate the fascinating mechanisms of charge excitation, separation, and transport in superlattice. We reiterate the photoexcitation discussed here is not the typical intermaterial electronic transition between VBM (BTO) and CBM (BFO) as reported in other oxides [57,135], because the spatial isolation of e and h channels in $(BaTiO_3)_4/(BiFeO_3)_{10}$ results in extremely weak overlap of electron wave functions between the band edge states. Under photoexcitation, first, the sublattices of $BaTiO_3$ and $BiFeO_3$ undergo their respective band edge transitions, i.e., $VBM_{BFO} \rightarrow CBM_{BFO}$ and $VBM_{BTO} \rightarrow CBM_{BTO}$ (Fig. 3 and Fig. S16 [21]). Second, the intrinsic

built-in potential drives the photoexcited e and h diffusing into their respective energy minima. For example, after photoexcitation in $BiFeO_3$ sublattice, the built-in potential drives e toward type-A interface and accumulates there, forming the e channel (blue) in $BiFeO_3$ side; it also drives h to move in an opposite direction, i.e., toward type-B interface, then across this $BaTiO_3/BiFeO_3$ interface entering the VB of $BaTiO_3$, and finally accumulates there, forming the h channel (red) in the $BaTiO_3$ side. A similar charge transport mechanism occurs in the $BaTiO_3$ side after photoexcitation. As a result, the e and h channels are spatially isolated in $BiFeO_3$ and $BaTiO_3$ respectively, while areas in between form a depletion channel that prohibits the presence of e or h (Fig. S14 [21]). Importantly, both e and h channels are parallel to interfaces (IP direction), resulting in CT orthogonal to charge-generation direction perpendicular to CS direction (z axis). Therefore, the CR during CT can be significantly suppressed, which is fundamentally different from both the conventional p-n [Fig. 1(a)] and BPV junctions [Fig. 1(b)].

Furthermore, this peculiar band alignment not only suppresses CR during transport, but also helps to maximize CS efficiency during charge generation. Driven by large interfacial band offsets, after forming a superlattice, the VBM and CBM of both $BiFeO_3$ and $BaTiO_3$ layers are significantly shifted at the band edges [Fig. 2(a) and Supplemental Material, Fig. S18(a) [21]]. The CS can be quantified by geometric DOS distribution of VBM and CBM near Fermi level, as illustrated in the inset of Fig. 4(a). Here we define the degree of e-h separation by estimating a DOS-related geometric factor [57], $R = \frac{1}{2} \{1 - [(M - M')/(M + M')]_{CBM} \times [(M - M')/(M + M')]_{VBM}\}$, where M and M' are integrated DOS of materials 1 and 2, respectively. The integration starts from
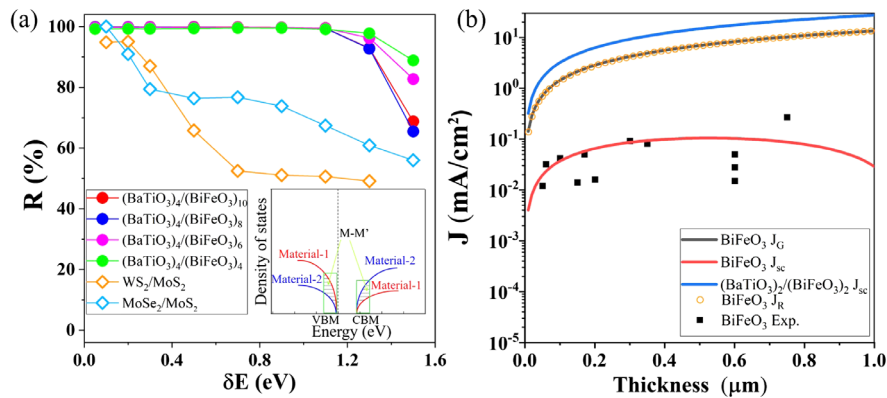

FIG. 4. (a) Calculated charge separation efficiency (R value) as a function of energy integration area for $(BaTiO_3)_4/(BiFeO_3)_n$ ($n = 4, 6, 8, 10$). R values of $MoSe_2/MoS_2$ [136] and WS_2/MoS_2 [137] are also included for direct comparison. Inset: illustrates definition of R value to estimate the charge separation by DOS [57], where M and M' are integrated DOS near the VBM or CBM for materials 1 and 2, respectively, and the integration begins from the VBM (CBM) to a lower (higher)-energy position within an energy range of δE. The dashed line is Fermi level. (b) Comparison of calculated various photocurrents J (J_{SC}, J_G, J_R) for $(BaTiO_3)_2/(BiFeO_3)_2$ superlattice and reference single $BiFeO_3$ based on macroscopic device simulations, along with experimental data obtained from Refs. [12,72,76–81,138–140].

the VBM (CBM) to a lower (higher) energy level within an energy range of δE ($0 < \delta E < 1.5$ eV). Therefore, R reflects the CS efficiency and $R \rightarrow 1$ indicates the CS efficiency approaching 100% with no recombination; i.e., material 1 (material 2) occupies 100% (0%) in VBM but 0% (100%) in CBM (VBM). Obviously, a more asymmetric occupation of DOS distribution in VBM and CBM leads to a larger R value, indicating more efficient CS. Figure 4(a) shows the calculated R values for different superlattices by varying energy integration range. Remarkably, the R values are close to unity for a very wide energy range up to 1.0 eV (Figs. S18 and S19 [21]), among the highest numbers in reported literatures [57,136,137] and significantly higher than that of vdW heterostructures of WS_2/MoS_2 and $MoSe_2/MoS_2$ [136,137]. Moreover, both e and h still coexist at band edges near the interface of $MoSe_2/MoS_2$, leading to unavoidable interlayer CR during CT. Therefore, we reiterate that the $(BaTiO_3)_m/(BiFeO_3)_n$ superlattices can achieve both ideal CS and CT without CR [Fig. 1(c)].

To clearly demonstrate the effect of CR suppression on the PV properties, we perform the macroscopic simulations using an equivalent ideal diode model illuminated under the solar radiation. The short-circuit current density (J_{SC}) of the system is defined as $J_{SC} = J_G - J_R$ [34,35], where J_G is the overall photocurrent generation upon on incident photon excitation and J_R is the dark current loss due to carrier recombination. Particularly, J_R involves the contributions from both nonradiative (J_R^{nr}) and radiative (J_R^r) processes. For the indirect-gap materials such as $BiFeO_3$, nonradiative recombination is usually a dominated loss mechanism and we also consider the radiative recombination by using a detailed-balance principle, assuming the emission rate and absorption rate through surface of cell are equal [43–45] (see Supplemental Material for simulation details for J_{SC}, J_G, J_R^{nr}, and J_R^r). As summarized in Fig. 4(b), for pure $BiFeO_3$, due to the significant nonradiative recombination, the obtained J_R is comparable to the magnitude order of photocurrent generation (J_G), resulting in a small J_{SC} (red curve), typically below 0.1 mA/cm^2. Importantly, our simulated J_{SC} values for $BiFeO_3$ as a function of absorber thickness are generally consistent with the experimentally measured ones for epitaxial films. The deviation between simulation and experimental values might reflect the extra recombination contribution from domain walls, which is not considered in our model but existed in the real $BiFeO_3$ systems. These results further suggest that, in pure $BiFeO_3$, strong carrier recombination is the limiting factor that restricts its potential for PV applications, which is confirmed by the prior experiments [52,138,141]. In contrast, the special electronic structure of $(BaTiO_3)_2/(BiFeO_3)_2$ superlattice quenches the CR, mainly because of spatial separation of carrier transport channels and the completely forbidden optical transitions around the superlattice band edges.

The stronger optical transitions in $BaTiO_3$ sublayers (see Fig. S16 and related discussion in [21]) and the eliminated CR can eventually result in an observed 2 orders of magnitude increase in J_{SC} (blue curve) for superlattice compared to that of $BiFeO_3$. Overall, the obtained J_{SC} for $BaTiO_3/BiFeO_3$ superlattice is on the order of a few mA/cm^2, which is still around one order of magnitude lower than mainstream semiconductors with narrower band gaps, e.g., compared to that of CdTe [9,44]. However, this level of photocurrent is one of the largest values among all the similar band gap materials, as shown in Fig. S20 in the Supplemental Material [21]. In addition, we also perform the first-principles photocurrent calculations to confirm our above simplified model calculations. As shown in Fig. S21 [21], the $(BaTiO_3)_4/(BiFeO_3)_4$ ultrathin film (in an ultrathin supercell) generally shows a significant enhancement of photocurrent than that of pure $BiFeO_3$, one qualitatively consistent with the macroscopic simulation results.

From practical device perspective, we note that the geometry of IP CT demonstrated in our $(BaTiO_3)_m/(BiFeO_3)_n$ shows an advantage in device setting, which has been achieved experimentally in epitaxial $BiFeO_3$ films [12,142,143]. For IP charge transport, electrodes can be fabricated at the edges of the device, i.e., left-right geometry, by routine lithography technique instead of traditional top-down electrodes. In this case, a top transparent conducting electrode is not a necessity, which can greatly help to simplify the device structure and associated efficiency loss.

Before concluding, we want to emphasize that the OCST band diagram we proposed is universal in many ferroelectric PD superlattices. For example, the $(SrTiO_3)_m/(BiFeO_3)_n$ and $(BaSnO_3)_m/(BiFeO_3)_n$ [see Fig. S22 [21]] can also exhibit a similar feature of built-in potential profile and CS phenomena to $(BaTiO_3)_m/(BiFeO_3)_n$, indicating that ideal CS and CT behaviors could also exist.

In summary, we propose a critical strategy to achieve superior CS efficiencies to maximum, which may potentially overcome the fundamental limitations in traditional p-n and BPV junctions. The OCST model, demonstrated in $(BaTiO_3)_m/(BiFeO_3)_n$ systems, can also achieve simultaneous high photocurrent with large band gap, suggesting more promising PV efficiencies than existing materials. Our work demonstrates a new idea to realize high-performance photon-to-electron conversions from a materials design perspective via artificial heterostructure engineering.

her help and support in offering resources in performing the photocurrent simulations.

*Corresponding author.
hyxiao@uestc.edu.cn
†Corresponding author.
Bing.Huang@csrc.ac.cn
‡Corresponding author.
liang.qiao@uestc.edu.cn

[1] S. K. Behura, C. Wang, Y. Wen, and V. Berry, Nat. Photonics **13**, 312 (2019).

[2] Q. Burlingame, X. H. Huang, X. Liu, C. Jeong, C. Coburn, and S. R. Forrest, Nature (London) **573**, 394 (2019).

[3] B. Shan, S. Vanka, T. T. Li, L. Troian-Gautier, M. K. Brennaman, Z. T. Mi, and T. J. Meyer, Nat. Energy **4**, 290 (2019).

[4] A. Kato and A. Ishizaki, Phys. Rev. Lett. **121**, 026001 (2018).

[5] L. Britnell, R. M. Ribeiro, A. Eckmann, R. Jalil, B. D. Belle, A. Mishchenko, Y. J. Kim, R. V. Gorbachev, T. Georgiou, S. V. Morozov, A. N. Grigorenko, A. K. Geim, C. Casiraghi, A. H. Castro Neto, and K. S. Novoselov, Science **340**, 1311 (2013).

[6] J. Kunstmann, F. Mooshammer, P. Nagler, A. Chaves, F. Stein, N. Paradiso, G. Plechinger, C. Strunk, C. Schuller, G. Seifert, D. R. Reichman, and T. Korn, Nat. Phys. **14**, 801 (2018).

[7] X. P. Hong, J. Kim, S. F. Shi, Y. Zhang, C. H. Jin, Y. H. Sun, S. Tongay, J. Q. Wu, Y. F. Zhang, and F. Wang, Nat. Nanotechnol. **9**, 682 (2014).

[8] U. Aeberhard and U. Rau, Phys. Rev. Lett. **118**, 247702 (2017).

[9] P. K. Nayak, S. Mahesh, H. J. Snaith, and D. Cahen, Nat. Rev. Mater. **4**, 269 (2019).

[10] G. Wang, A. Chernikov, M. M. Glazov, T. F. Heinz, X. Marie, T. Amand, and B. Urbaszek, Rev. Mod. Phys. **90**, 021001 (2018).

[11] T. Choi, S. Lee, Y. J. Choi, V. Kiryukhin, and S. W. Cheong, Science **324**, 63 (2009).

[12] S. Y. Yang, J. Seidel, S. J. Byrnes, P. Shafer, C. H. Yang, M. D. Rossell, P. Yu, Y. H. Chu, J. F. Scott, J. W. Ager, III, L. W. Martin, and R. Ramesh, Nat. Nanotechnol. **5**, 143 (2010).

[13] R. Nechache, C. Harnagea, S. Li, L. Cardenas, W. Huang, J. Chakrabartty, and F. Rosei, Nat. Photonics **9**, 61 (2015).

[14] A. Zenkevich, Y. Matveyev, K. Maksimova, R. Gaynutdinov, A. Tolstikhina, and V. Fridkin, Phys. Rev. B **90**, 161409(R) (2014).

[15] S. M. Young and A. M. Rappe, Phys. Rev. Lett. **109**, 116601 (2012).

[16] A. Bhatnagar, Y. H. Kim, D. Hesse, and M. Alexe, Nano Lett. **14**, 5224 (2014).

[17] J. J. Plata, J. A. Suarez, S. Cuesta-Lopez, A. M. Marquez, and J. F. Sanz, J. Mater. Chem. A **7**, 27323 (2019).

[18] L. Jiang, I. Grinberg, F. G. Wang, S. M. Young, P. K. Davies, and A. M. Rappe, Phys. Rev. B **90**, 075153 (2014).

[19] J. J. Plata, A. M. Marquez, S. Cuesta-Lopez, and J. F. Sanz, Acta Mater. **204**, 116466 (2021).

[20] F. G. Wang, I. Grinberg, and A. M. Rappe, Appl. Phys. Lett. **104**, 152903 (2014).

[21] See the Supplemental Material at http://link.aps.org/supplemental/10.1103/PhysRevLett.126.176401 for the details of theoretical methods, electronic structures, and optical transitions of different ferroelectric oxide super-lattices, the calculated photocurrents, discussion of spontaneous polarization and built-in polarization, charge separation efficiency and ferroelectric polarization, and diagram of band gap photocurrent of different semiconductors, which includes Refs. [12–15,22–128].

[22] P. E. Blochl, Phys. Rev. B **50**, 17953 (1994).

[23] G. Kresse and J. Hafner, Phys. Rev. B **47**, 558 (1993).

[24] J. P. Perdew, K. Burke, and M. Ernzerhof, Phys. Rev. Lett. **77**, 3865 (1996).

[25] H. Matsuo, Y. Kitanaka, R. Inoue, Y. Noguchi, and M. Miyayama, Jpn. J. Appl. Phys. **54**, 10NA03 (2015).

[26] L. Qiao, S. Zhang, H. Y. Xiao, D. J. Singh, K. H. L. Zhang, Z. J. Liu, X. T. Zu, and S. Li, J. Mater. Chem. C **6**, 1239 (2018).

[27] J. B. Neaton, C. Ederer, U. V. Waghmare, N. A. Spaldin, and K. M. Rabe, Phys. Rev. B **71**, 014113 (2005).

[28] M. Shishkin and G. Kresse, Phys. Rev. B **74**, 035101 (2006).

[29] M. Shishkin and G. Kresse, Phys. Rev. B **75**, 235102 (2007).

[30] S. Albrecht, L. Reining, R. Del Sole, and G. Onida, Phys. Rev. Lett. **80**, 4510 (1998).

[31] M. Rohlfing and S. G. Louie, Phys. Rev. Lett. **81**, 2312 (1998).

[32] J. Taylor, H. Guo, and J. Wang, Phys. Rev. B **63**, 245407 (2001).

[33] J. Z. Chen, Y. B. Hu, and H. Guo, Phys. Rev. B **85**, 155441 (2012).

[34] A. Niv, M. Gharghi, C. Gladden, O. D. Miller, and X. Zhang, Phys. Rev. Lett. **109**, 138701 (2012).

[35] J. Y. Wu, J. Luke, H. K. H. Lee, P. S. Tuladhar, H. Cha, S. Y. Jang, W. C. Tsoi, M. Heeney, H. Kang, K. Lee, T. Kirchartz, J. S. Kim, and J. R. Durrant, Nat. Commun. **10**, 5159 (2019).

[36] B. Godefroid and G. Kozyreff, Phys. Rev. Applied **8**, 034024 (2017).

[37] R. Brenes, M. Laitz, J. Jean, D. W. deQuilettes, and V. Bulovic, Phys. Rev. Applied **12**, 014017 (2019).

[38] C. Wehrenfennig, G. E. Eperon, M. B. Johnston, H. J. Snaith, and L. M. Herz, Adv. Mater. **26**, 1584 (2014).

[39] L. J. A. Koster, O. Stenzel, S. D. Oosterhout, M. M. Wienk, V. Schmidt, and R. A. J. Janssen, Adv. Energy Mater. **3**, 615 (2013).

[40] M. M. Mandoc, L. J. A. Koster, and P. W. M. Blom, Appl. Phys. Lett. **90**, 133504 (2007).

[41] L. J. A. Koster, E. C. P. Smits, V. D. Mihailetchi, and P. W. M. Blom, Phys. Rev. B **72**, 085205 (2005).

[42] D. Bi, W. Tress, M. I. Dar, P. Gao, J. Luo, C. Renevier, K. Schenk, A. Abate, F. Giordano, J.-P. C. Baena, J.-D. Decoppet, S. M. Zakeeruddin, M. K. Nazeeruddin, M. Gratzel, and A. Hagfeldt, Sci. Adv. **2**, e1501170 (2016).

[43] U. Rau, Phys. Rev. B **76**, 085303 (2007).
[44] X. Huang, T. R. Paudel, S. Dong, and E. Y. Tsymbal, Phys. Rev. B **92**, 125201 (2015).
[45] J. H. Werner, S. Kolodinski, and H. J. Queisser, Phys. Rev. Lett. **72**, 3851 (1994).
[46] Y. Zang, D. Xie, Y. Chen, X. Wu, T. Ren, J. Wei, H. Zhu, and D. Plant, Nanoscale **4**, 2926 (2012).
[47] J. G. Wu, J. Wang, D. Q. Xiao, and J. G. Zhu, ACS Appl. Mater. Interfaces **3**, 3261 (2011).
[48] J. C. Yang, C. H. Yeh, Y. T. Chen, S. C. Liao, R. Huang, H. J. Liu, C. C. Hung, S. H. Chen, S. L. Wu, C. H. Lai, Y. P. Chiu, P. W. Chiu, and Y. H. Chu, Nanoscale **6**, 10524 (2014).
[49] A. Anshul, A. Kumar, B. K. Gupta, R. K. Kotnala, J. F. Scott, and R. S. Katiyar, Appl. Phys. Lett. **102**, 222901 (2013).
[50] M. M. Yang, A. N. Iqbal, J. J. P. Peters, A. M. Sanchez, and M. Alexe, Nat. Commun. **10**, 2791 (2019).
[51] J. C. Yang, Q. He, P. Yu, and Y. H. Chu, Annu. Rev. Mater. Res. **45**, 249 (2015).
[52] L. You, F. Zheng, L. Fang, Y. Zhou, L. Z. Tan, Z. Zhang, G. Ma, D. Schmidt, A. Rusydi, L. Wang, L. Chang, A. M. Rappe, and J. Wang, Sci. Adv. **4**, eaat3438 (2018).
[53] S. Hunpratub, P. Thongbai, T. Yamwong, R. Yimnirun, and S. Maensiri, Appl. Phys. Lett. **94**, 062904 (2009).
[54] Y. Y. Zang, D. Xie, X. Wu, Y. Chen, Y. X. Lin, M. H. Li, H. Tian, X. Li, Z. Li, H. W. Zhu, T. L. Ren, and D. Plant, Appl. Phys. Lett. **99**, 132904 (2011).
[55] C. J. Cheng, D. Kan, V. Anbusathaiah, I. Takeuchi, and V. Nagarajan, Appl. Phys. Lett. **97**, 212905 (2010).
[56] S. Y. Yang, L. W. Martin, S. J. Byrnes, T. E. Conry, S. R. Basu, D. Paran, L. Reichertz, J. Ihlefeld, C. Adamo, A. Melville, Y. H. Chu, C. H. Yang, J. L. Musfeldt, D. G. Schlom, J. W. Ager, and R. Ramesh, Appl. Phys. Lett. **95**, 062909 (2009).
[57] D. Kim, H. Han, J. H. Lee, J. W. Choi, J. C. Grossman, H. M. Jang, and D. Kim, Proc. Natl. Acad. Sci. U.S.A. **115**, 6566 (2018).
[58] J. K. Shenton, D. R. Bowler, and W. L. Cheah, Phys. Rev. B **100**, 085120 (2019).
[59] N. Nakagawa, H. Y. Hwang, and D. A. Muller, Nat. Mater. **5**, 204 (2006).
[60] S. M. Nakhmanson, K. M. Rabe, and D. Vanderbilt, Appl. Phys. Lett. **87**, 102906 (2005).
[61] C. Ederer and N. A. Spaldin, Phys. Rev. Lett. **95**, 257601 (2005).
[62] J. X. Zhang, Q. He, M. Trassin, W. Luo, D. Yi, M. D. Rossell, P. Yu, L. You, C. H. Wang, C. Y. Kuo, J. T. Heron, Z. Hu, R. J. Zeches, H. J. Lin, A. Tanaka, C. T. Chen, L. H. Tjeng, Y. H. Chu, and R. Ramesh, Phys. Rev. Lett. **107**, 147602 (2011).
[63] Y. Wang, M. K. Niranjan, S. S. Jaswal, and E. Y. Tsymbal, Phys. Rev. B **80**, 165130 (2009).
[64] O. Nakagawara, T. Shimuta, T. Makino, S. Arai, H. Tabata, and T. Kawai, Vacuum **66**, 397 (2002).
[65] W. Zhong, D. Vanderbilt, and K. M. Rabe, Phys. Rev. Lett. **73**, 1861 (1994).
[66] R. Ranjith, U. Lüders, and W. Prellier, J Phys. Chem. Solids **71**, 1140 (2010).

[67] Y. F. Hou, W. L. Li, T. D. Zhang, W. Wang, W. P. Cao, X. L. Liuc, and W. D. Fei, Phys. Chem. Chem. Phys. **17**, 11593 (2015).
[68] C. Himcinschi, A. Bhatnagar, A. Talkenberger, M. Barchuk, D. R. T. Zahn, D. Rafaja, J. Kortus, and M. Alexe, Appl. Phys. Lett. **106**, 012908 (2015).
[69] P. Chen, N. J. Podraza, X. S. Xu, A. Melville, E. Vlahos, V. Gopalan, R. Ramesh, D. G. Schlom, and J. L. Musfeldt, Appl. Phys. Lett. **96**, 131907 (2010).
[70] D. Schmidt, L. You, X. Chi, J. Wang, and A. Rusydi, Phys. Rev. B **92**, 075310 (2015).
[71] Y. F. Cui, J. Briscoe, Y. Q. Wang, N. V. Tarakina, and S. Dunn, ACS Appl. Mater. Interfaces **9**, 24518 (2017).
[72] S. Sharma, M. Tomar, A. Kumar, N. K. Puri, and V. Gupta, J. Appl. Phys. **118**, 074103 (2015).
[73] M. Alexe and D. Hesse, Nat. Commun. **2**, 256 (2011).
[74] H. Matsuo, Y. Noguchi, and M. Miyayama, Nat. Commun. **8**, 207 (2017).
[75] P. Machado, M. Scigaj, J. Gazquez, E. Rueda, A. Sanchez-Diaz, I. Fina, M. Gibert-Roca, T. Puig, X. Obradors, M. Campoy-Quiles, and M. Coll, Chem. Mater. **31**, 947 (2019).
[76] W. Ji, K. Yao, and Y. C. Liang, Adv. Mater. **22**, 1763 (2010).
[77] J. H. Shah, H. Ye, Y. Liu, A. M. Idris, A. S. Malik, Y. Zhang, H. Han, and C. Li, J. Mater. Chem. A **8**, 6863 (2020).
[78] F. Wu, Y. Guo, B. Guo, Y. Zhang, H. Li, and H. Liu, J Phys. D **46**, 365304 (2013).
[79] J. Chakrabartty, R. Nechache, C. Harnagea, S. Li, and F. Rosei, Nanotechnology **27**, 215402 (2016).
[80] R. K. Katiyar, P. Misra, F. Mendoza, G. Morell, and R. S. Katiyar, Appl. Phys. Lett. **105**, 142902 (2014).
[81] Z. Fan, K. Yao, and J. Wang, Appl. Phys. Lett. **105**, 162903 (2014).
[82] L. F. Wang, Y. F. Li, A. Bera, C. Ma, F. Jin, K. D. Yuan, W. J. Yin, A. David, W. Chen, W. B. Wu, W. Prellier, S. H. Wei, and T. Wu, Phys. Rev. Applied **3**, 064015 (2015).
[83] M. Nakamura, F. Kagawa, T. Tanigaki, H. S. Park, T. Matsuda, D. Shindo, Y. Tokura, and M. Kawasaki, Phys. Rev. Lett. **116**, 156801 (2016).
[84] J. Chakrabartty, C. Harnagea, M. Celikin, F. Rosei, and R. Nechache, Nat. Photonics **12**, 271 (2018).
[85] W. Dong, Y. P. Guo, B. Guo, H. Li, H. Z. Liu, and T. W. Joel, ACS Appl. Mater. Interfaces **5**, 6925 (2013).
[86] I. Grinberg, D. V. West, M. Torres, G. Y. Gou, D. M. Stein, L. Y. Wu, G. N. Chen, E. M. Gallo, A. R. Akbashev, P. K. Davies, J. E. Spanier, and A. M. Rappe, Nature (London) **503**, 509 (2013).
[87] F. Han, Y. J. Zhang, C. L. Yuan, X. Liu, B. H. Zhu, F. Liu, J. W. Xu, C. R. Zhou, J. Wang, and G. H. Rao, Ceram. Int. **46**, 14567 (2020).
[88] S. Li, J. M. Zhang, B. P. Zhang, W. Huang, C. Harnagea, R. Nechache, L. F. Zhu, S. W. Zhang, Y. H. Lin, L. Ni, Y. H. Sang, H. Liu, and F. Rosei, Nano Energy **35**, 92 (2017).
[89] D. F. Yu, Z. H. Liu, J. M. Zhang, S. Li, Z. C. Zhao, L. F. Zhu, W. S. Liu, Y. H. Lin, H. Liu, and Z. T. Zhang, Nano Energy **58**, 695 (2019).

[90] F. G. Zheng, Y. Xin, W. Huang, J. X. Zhang, X. F. Wang, M. R. Shen, W. Dong, L. Fang, Y. B. Bai, X. Q. Shen, and J. H. Hao, J. Mater. Chem. A **2**, 1363 (2014).

[91] D. W. Cao, C. Y. Wang, F. G. Zheng, W. Dong, L. Fang, and M. R. Shen, Nano Lett. **12**, 2803 (2012).

[92] M. Qin, K. Yao, and Y. C. Liang, Appl. Phys. Lett. **93**, 122904 (2008).

[93] J. J. Zhang, X. D. Su, M. R. Shen, Z. H. Shen, L. J. Zhang, X. Y. Zhang, W. X. Cheng, M. Y. Cao, and G. Zou, Sci. Rep. **3**, 2109 (2013).

[94] T. Choi, L. Jiang, S. Lee, T. Egami, and H. N. Lee, New J. Phys. **14**, 093056 (2012).

[95] W. C. Xiang, Z. W. Wang, D. J. Kubicki, W. Tress, J. S. Luo, D. Prochowicz, S. Akin, L. Emsley, J. T. Zhou, G. Dietler, M. Gratzel, and A. Hagfeldt, Joule **3**, 205 (2019).

[96] C. F. J. Lau, X. F. Deng, Q. S. Ma, J. H. Zheng, J. S. Yun, M. A. Green, S. J. Huang, and A. W. Y. Ho-Baillie, ACS Energy Lett. **1**, 573 (2016).

[97] Y. C. Shih, L. Y. Wang, H. C. Hsieh, and K. F. Lin, J. Mater. Chem. A **3**, 9133 (2015).

[98] S. G. Motti, D. Meggiolaro, A. J. Barker, E. Mosconi, C. A. R. Perini, J. M. Ball, M. Gandini, M. Kim, F. De Angelis, and A. Petrozza, Nat. Photonics **13**, 532 (2019).

[99] J. W. Lee, D. J. Seol, A. N. Cho, and N. G. Park, Adv. Mater. **26**, 4991 (2014).

[100] N. Blouin, A. Michaud, and M. Leclerc, Adv. Mater. **19**, 2295 (2007).

[101] S. H. Park, A. Roy, S. Beaupre, S. Cho, N. Coates, J. S. Moon, D. Moses, M. Leclerc, K. Lee, and A. J. Heeger, Nat. Photonics **3**, 297 (2009).

[102] Y. Kim, S. Cook, S. M. Tuladhar, S. A. Choulis, J. Nelson, J. R. Durrant, D. D. C. Bradley, M. Giles, I. McCulloch, C. S. Ha, and M. Ree, Nat. Mater. **5**, 197 (2006).

[103] M. L. Bohm, T. C. Jellicoe, M. Tabachnyk, N. Davis, F. Wisnivesky-Rocca-Rivarola, C. Ducati, B. Ehrler, A. A. Bakulin, and N. C. Greenham, Nano Lett. **15**, 7987 (2015).

[104] P. H. Rekemeyer, S. Chang, C. H. M. Chuang, G. W. Hwang, M. G. Bawendi, and S. Gradecak, Adv. Energy Mater. **6**, 1600848 (2016).

[105] K. Y. Lu, Y. J. Wang, J. Y. Yuan, Z. Q. Cui, G. Z. Shi, S. H. Shi, L. Han, S. Chen, Y. N. Zhang, X. F. Ling, Z. K. Liu, L. F. Chi, J. Fan, and W. L. Ma, J. Mater. Chem. A **5**, 23960 (2017).

[106] L. Etgar, D. Yanover, R. K. Capek, R. Vaxenburg, Z. S. Xue, B. Liu, M. K. Nazeeruddin, E. Lifshitz, and M. Gratzel, Adv. Funct. Mater. **23**, 2736 (2013).

[107] O. E. Semonin, J. M. Luther, and M. C. Beard, Mater. Today **15**, 508 (2012).

[108] G. Mariani, P. S. Wong, A. M. Katzenmeyer, F. Leonard, J. Shapiro, and D. L. Huffaker, Nano Lett. **11**, 2490 (2011).

[109] J. P. Boulanger, A. C. E. Chia, B. Wood, S. Yazdi, T. Kasama, M. Aagesen, and R. R. LaPierre, IEEE J. Photovoltaics **6**, 661 (2016).

[110] G. Mariani, A. C. Scofield, C. H. Hung, and D. L. Huffaker, Nat. Commun. **4**, 1497 (2013).

[111] G. Mariani, Z. L. Zhou, A. Scofield, and D. L. Huffaker, Nano Lett. **13**, 1632 (2013).

[112] M. Q. Yao, N. F. Huang, S. Cong, C. Y. Chi, M. A. Seyedi, Y. T. Lin, Y. Cao, M. L. Povinelli, P. D. Dapkus, and C. W. Zhou, Nano Lett. **14**, 3293 (2014).

[113] K. Yoshikawa, H. Kawasaki, W. Yoshida, T. Irie, K. Konishi, K. Nakano, T. Uto, D. Adachi, M. Kanematsu, H. Uzu, and K. Yamamoto, Nat. Energy **2**, 17032 (2017).

[114] M. A. Green, E. D. Dunlop, D. H. Levi, J. Hohl-Ebinger, M. Yoshita, and A. W. Y. Ho-Baillie, Prog. Photovoltaics **27**, 565 (2019).

[115] P. K. Mohseni, A. Behnam, J. D. Wood, X. Zhao, K. J. Yu, N. C. Wang, A. Rockett, J. A. Rogers, J. W. Lyding, E. Pop, and X. L. Li, Adv. Mater. **26**, 3755 (2014).

[116] A. Nowzari, M. Heurlin, V. Jain, K. Storm, A. Hosseinnia, N. Anttu, M. T. Borgstrom, H. Pettersson, and L. Samuelson, Nano Lett. **15**, 1809 (2015).

[117] Y. Cui, J. Wang, S. R. Plissard, A. Cavalli, T. T. T. Vu, R. P. J. van Veldhoven, L. Gao, M. Trainor, M. A. Verheijen, J. E. M. Haverkort, and E. P. A. M. Bakkers, Nano Lett. **13**, 4113 (2013).

[118] J. Wallentin, N. Anttu, D. Asoli, M. Huffman, I. Aberg, M. H. Magnusson, G. Siefer, P. Fuss-Kailuweit, F. Dimroth, B. Witzigmann, H. Q. Xu, L. Samuelson, K. Deppert, and M. T. Borgstrom, Science **339**, 1057 (2013).

[119] N. E. Gorji, U. Reggiani, and L. Sandrolini, Sol. Enegy **86**, 920 (2012).

[120] J. M. Burst, J. N. Duenow, D. S. Albin, E. Colegrove, M. O. Reese, J. A. Aguiar, C. S. Jiang, M. K. Patel, M. M. Al-Jassim, D. Kuciauskas, S. Swain, T. Ablekim, K. G. Lynn, and W. K. Metzger, Nat. Energy **1**, 16015 (2016).

[121] Y. Zhao, M. Boccard, S. Liu, J. Becker, X. H. Zhao, C. M. Campbell, E. Suarez, M. B. Lassise, Z. Holman, and Y. H. Zhang, Nat. Energy **1**, 16067 (2016).

[122] J. D. Major, R. E. Treharne, L. J. Phillips, and K. Durose, Nature (London) **511**, 334 (2014).

[123] M. Bernechea, N. C. Miller, G. Xercavins, D. So, A. Stavrinadis, and G. Konstantatos, Nat. Photonics **10**, 521 (2016).

[124] L. Wang, D. B. Li, K. H. Li, C. Chen, H. X. Deng, L. Gao, Y. Zhao, F. Jiang, L. Y. Li, F. Huang, Y. S. He, H. S. Song, G. D. Niu, and J. Tang, Nat. Energy **2**, 17046 (2017).

[125] Y. Zhou, L. Wang, S. Y. Chen, S. K. Qin, X. S. Liu, J. Chen, D. J. Xue, M. Luo, Y. Z. Cao, Y. B. Cheng, E. H. Sargent, and J. Tang, Nat. Photonics **9**, 409 (2015).

[126] J. B. Li, V. Chawla, and B. M. Clemens, Adv. Mater. **24**, 720 (2012).

[127] T. K. Todorov, K. B. Reuter, and D. B. Mitzi, Adv. Mater. **22**, E156 (2010).

[128] W. Wang, M. T. Winkler, O. Gunawan, T. Gokmen, T. K. Todorov, Y. Zhu, and D. B. Mitzi, Adv. Energy Mater. **4**, 1301465 (2014).

[129] A. Ohtomo and H. Y. Hwang, Nature (London) **427**, 423 (2004).

[130] S. A. Chambers, L. Qiao, T. C. Droubay, T. C. Kaspar, B. W. Arey, and P. V. Sushko, Phys. Rev. Lett. **107**, 206802 (2011).

[131] L. Qiao, K. H. L. Zhang, M. E. Bowden, T. Varga, V. Shutthanandan, R. Colby, Y. Du, B. Kabius, P. V. Sushko, M. D. Biegalski, and S. A. Chambers, Adv. Funct. Mater. **23**, 2953 (2013).

[132] M. M. Ugeda, A. J. Bradley, S. F. Shi, F. H. da Jornada, Y. Zhang, D. Y. Qiu, W. Ruan, S. K. Mo, Z. Hussain, Z. X.

Shen, F. Wang, S. G. Louie, and M. F. Crommie, Nat. Mater. **13**, 1091 (2014).

[133] J. Liu, S. Okamoto, M. van Veenendaal, M. Kareev, B. Gray, P. Ryan, J. W. Freeland, and J. Chakhalian, Phys. Rev. B **83**, 161102(R) (2011).

[134] Y. Ando, G. S. Boebinger, A. Passner, N. L. Wang, C. Geibel, and F. Steglich, Phys. Rev. Lett. **77**, 2065 (1996).

[135] L. Qiao, H. Y. Xiao, H. M. Meyer, J. N. Sun, C. M. Rouleau, A. A. Puretzky, D. B. Geohegan, I. N. Ivanov, M. Yoon, W. J. Weber, and M. D. Biegalski, J. Mater. Chem. C **1**, 4628 (2013).

[136] R. Long and O. V. Prezhdo, Nano Lett. **16**, 1996 (2016).

[137] L. Q. Li, R. Long, and O. V. Prezhdo, Chem. Mater. **29**, 2466 (2017).

[138] J. Song, T. L. Kim, J. Lee, S. Y. Cho, J. Cha, S. Y. Jeong, H. An, W. S. Kim, Y.-S. Jung, J. Park, G. Y. Jung, D.-Y. Kim, J. Y. Jo, S. D. Bu, H. W. Jang, and S. Lee, Nano. Res. **11**, 642 (2018).

[139] Z. Peng, Y. Wang, and B. Liu, Mater. Sci. Semicond. Process. **35**, 115 (2015).

[140] V. Keskin, A. Gupta, and G. Szulczewski, Mater. Lett. **159**, 305 (2015).

[141] L. Wang, H. Ma, L. Chang, C. Ma, G. Yuan, J. Wang, and T. Wu, Small **13**, 1602355 (2017).

[142] W. Ji, K. Yao, and Y. C. Liang, Phys. Rev. B **84**, 094115 (2011).

[143] B. Guzelturk, A. B. Mei, L. Zhang, L. Z. Tan, P. Donahue, A. G. Singh, D. G. Schlom, L. W. Martin, and A. M. Lindenberg, Nano Lett. **20**, 145 (2020).